

MIT Open Access Articles

Generation of coherent phonons by coherent extreme ultraviolet radiation in a transient grating experiment

The MIT Faculty has made this article openly available. **Please share** how this access benefits you. Your story matters.

Citation: Maznev, A. A. et al. "Generation of coherent phonons by coherent extreme ultraviolet radiation in a transient grating experiment." Applied Physics Letters 113, 22 (November 2018): 221905 © 2018 Author(s)

As Published: <http://dx.doi.org/10.1063/1.5048023>

Publisher: AIP Publishing

Persistent URL: <https://hdl.handle.net/1721.1/123536>

Version: Final published version: final published article, as it appeared in a journal, conference proceedings, or other formally published context







Terms of Use: Article is made available in accordance with the publisher's policy and may be subject to US copyright law. Please refer to the publisher's site for terms of use.



Generation of coherent phonons by coherent extreme ultraviolet radiation in a transient grating experiment

Cite as: Appl. Phys. Lett. **113**, 221905 (2018); <https://doi.org/10.1063/1.5048023>

Submitted: 10 July 2018 . Accepted: 09 November 2018 . Published Online: 27 November 2018

A. A. Maznev, F. Bencivenga , A. Cannizzo, F. Capotondi, R. Cucini , R. A. Duncan, T. Feuer, T. D. Frazer , L. Foglia , H.-M. Frey, H. Kapteyn, J. Knobloch, G. Knopp, C. Masciovecchio, R. Mincigrucci, G. Monaco, M. Murnane, I. Nikolov, E. Pedersoli , A. Simoncig, A. Vega-Flick , and K. A. Nelson



View Online



Export Citation



CrossMark

ARTICLES YOU MAY BE INTERESTED IN

[Integration of quantum dots with lithium niobate photonics](#)

Applied Physics Letters **113**, 221102 (2018); <https://doi.org/10.1063/1.5054865>

[Nonlinear XUV-optical transient grating spectroscopy at the Si L_{2,3}-edge](#)

Applied Physics Letters **114**, 181101 (2019); <https://doi.org/10.1063/1.5085413>

[Frequency-selective excitation of high-wavevector phonons](#)

Applied Physics Letters **113**, 171901 (2018); <https://doi.org/10.1063/1.5047447>

Applied Physics Letters

Mid-IR and THz frequency combs
special collection

[Read Now!](#)

AIP
Publishing

Generation of coherent phonons by coherent extreme ultraviolet radiation in a transient grating experiment

A. A. Maznev,^{1,a)} F. Bencivenga,² A. Cannizzo,³ F. Capotondi,² R. Cucini,^{2,4} R. A. Duncan,¹ T. Feuer,³ T. D. Frazer,⁵ L. Foglia,² H.-M. Frey,³ H. Kapteyn,⁵ J. Knobloch,⁵ G. Knopp,⁶ C. Masciovecchio,² R. Mincigrucci,² G. Monaco,⁷ M. Murnane,⁵ I. Nikolov,² E. Pedersoli,² A. Simoncig,² A. Vega-Flick,⁸ and K. A. Nelson¹

¹Massachusetts Institute of Technology, Cambridge, Massachusetts 02139, USA

²Elettra Sincrotrone Trieste S.C.p.A, 34149 Basovizza, TS, Italy

³Institute of Applied Physics, University of Bern, 3012 Bern, Switzerland

⁴Istituto Officina dei Materiali CNR, 34149 Basovizza, TS, Italy

⁵JILA and Department of Physics, University of Colorado, Boulder, Colorado 80309, USA

⁶Paul Scherrer Institute, Villigen 5232, Switzerland

⁷Department of Physics, University of Trento, I-38123 Povo, TN, Italy

⁸Applied Physics Department, CINVESTAV-Unidad Mérida, Mérida, Yucatán 97310, Mexico

(Received 10 July 2018; accepted 9 November 2018; published online 27 November 2018)

We investigate the excitation of coherent acoustic and optical phonons by ultrashort extreme ultraviolet (EUV) pulses produced by a free electron laser. Two crossed femtosecond EUV (wavelength 12.7 nm) pulses are used to excite coherent phonons at a wavelength of 280 nm, which are detected via diffraction of an optical probe beam. Longitudinal and surface acoustic waves are measured in BK-7 glass, diamond, and Bi₄Ge₃O₁₂; in the latter material, the excitation of a coherent optical phonon mode is also observed. We discuss probing different acoustic modes in reflection and transmission geometries and frequency mixing of surface and bulk acoustic waves in the signal. The use of extreme ultraviolet radiation will allow the creation of tunable GHz to THz acoustic sources in any material without the need to fabricate transducer structures. *Published by AIP Publishing.* <https://doi.org/10.1063/1.5048023>

In the past decade, remarkable progress has been achieved in developing ultrafast extreme ultraviolet (EUV) and x-ray sources,¹ which have already yielded many breakthroughs in different fields of science. In time-resolved studies of condensed matter, short-wavelength radiation is typically used to probe dynamics initiated by a femtosecond optical pulse. In particular, ultrafast x-ray diffraction has been used to probe acoustic^{2–5} and optical^{6,7} coherent phonons (meaning lattice vibrations with a well-defined phase), whereas x-ray diffuse scattering has been employed to probe the dynamics of parametrically driven squeezed phonon populations.⁸ Femtosecond EUV pulses have also been used to detect high frequency surface acoustic waves (SAWs).^{9,10} In all these studies, short-wavelength radiation was used to probe lattice dynamics excited by optical laser pulses. High brightness EUV and x-ray free electron lasers (FELs) now allow experiments in which femtosecond short-wavelength pulses are used to *initiate* dynamics probed with optical or short-wavelength radiation.^{11–17} This report is aimed at exploring the potential of short-wavelength photon pulses for the excitation of lattice vibrations.

An effective approach to generate tunable coherent phonons by light is the transient grating (TG) technique,^{18–20} which can be regarded as a third order wave-mixing process. In this method, widely used in both fundamental and applied research,^{21–24} two coherent pulses crossed in the sample form an optical interference pattern with a spatial period

$\Lambda = \lambda/2 \sin(\theta)$, where λ is the wavelength and 2θ is the angle between the two beams. The interaction of the radiation with the medium, via various mechanisms, generates coherent phonons at the wavelength equal to Λ , which are detected via diffraction of a probe laser beam. The phonon wavevector can be tuned by changing the angle θ ; however, it cannot be made shorter than $\lambda/2$. In practice, the shortest TG period achieved with optical excitation was $\sim 0.5 \mu\text{m}$.²⁵ The potential of the TG technique would be greatly enhanced by extending it into the nanometer range of phonon wavelengths, where many interesting and technologically relevant phonon physics phenomena take place (for example, most of the heat in non-metallic solids is carried by nanometer-wavelength phonons).

Recently, a dedicated effort on implementing an EUV TG setup at the fully coherent FEL source FERMI (Elettra, Trieste, Italy)²⁶ enabled the observation of EUV-excited TG responses^{12,26} probed by optical pulses. These initial experiments mainly focused on the electronic response decaying within ~ 1 ps following the excitation, while the presence of a coherent phonon signal was only tentatively suggested.¹² In this report, we use the TG setup at FERMI to unambiguously demonstrate the generation of bulk and surface coherent acoustic phonons as well as coherent optical phonons by femtosecond EUV pulses.

The experiments were performed at the DiProI beamline at FERMI²⁷ with the apparatus described in detail in Ref. 26, which we modified by adding the reflection mode measurement capability, see Fig. 1. The stable operation of the FERMI FEL2 source²⁸ at 50 Hz, with shot-to-shot flux fluctuations

^{a)}Author to whom correspondence should be addressed: alexei.maznev@gmail.com

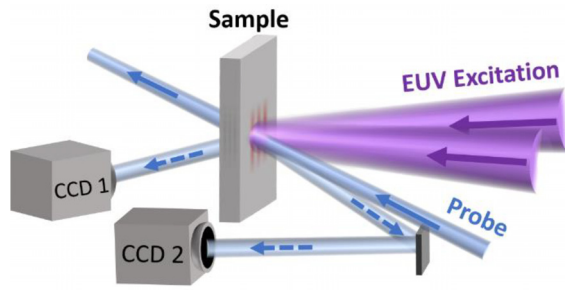


FIG. 1. Schematic of the experiment. Two 12.7 nm EUV pulses launch coherent phonons producing a transient diffraction grating in the sample, which is monitored via diffraction of a time-delayed 400 nm probe pulse. Diffracted probe beams (dashed arrows) are detected by CCD cameras.

$\sim 15\%$, contributed to the improved data quality compared to prior work.^{12,26} Two time-coincident 70 fs EUV pulses at a wavelength of 12.7 nm and with a total energy of $3 \mu\text{J}$ are crossed at the sample at the angle $2\theta = 2.62^\circ$ (set with $\sim 2\%$ accuracy) forming an interference pattern with the period $\Lambda = 277 \text{ nm}$. The seeded FERMI FEL yields excellent transverse and longitudinal coherence, with EUV pulses being nearly transform-limited,²⁸ which ensures high contrast of the interference pattern within the entire $100 \mu\text{m}$ EUV spot.²⁹ The EUV radiation absorbed by the sample generates coherent phonons at the wavelength Λ , which modulate the refractive index (and also, in the case of surface acoustic phonons, the surface displacement). The spatially sinusoidal refractive index variation acts as a transient diffraction grating for the time-delayed 400 nm 100 fs probe pulse. Both pumps and probe are S polarized. The probe beam is incident at an angle of 46° to the sample normal determined from the Bragg diffraction condition; however, since the EUV penetration depth is small ($\sim 100 \text{ nm}$ for diamond and BK-7, and 28 nm for BGO³⁰), transient gratings are thin and the Bragg angle incidence is not strictly required. The diffracted probe beam is detected by a CCD camera denoted CCD1. Since the TG is produced at the sample surface, it also acts as a reflecting diffraction grating. The probe beam diffracted in reflection is picked up by a mirror and detected by the second camera CCD2. The sample is slightly tilted so that the back-diffracted beam goes below the incident probe beam. Additional optics (two lenses and an aperture) not shown in the figure are inserted between the mirror and CCD2 in order to reduce the spot size on the camera and filter out stray light. At each pump-probe delay, the signal is averaged over 600–2000 FEL shots. (It took a few hours to measure each of the signal waveforms shown below.) All samples are double-polished plates with thickness over 0.5 mm, i.e., much greater than both the EUV absorption depth and the TG period.

Figures 2(a) and 2(b) show the diffraction signal as a function of the pump-probe delay measured on the single crystal diamond sample in the transmission geometry. The surface orientation of the sample was (001), with the TG wavevector aligned along [110]. The signal appears after the arrival of the excitation EUV pulses at $t = 0$ and is initially dominated by an intense peak with a decay time of 1.2 ps, which we ascribe to an electronic response. This is followed by a slower decay with a few irregular oscillations; finally, after $\sim 75 \text{ ps}$ we see a regular oscillation pattern shown in

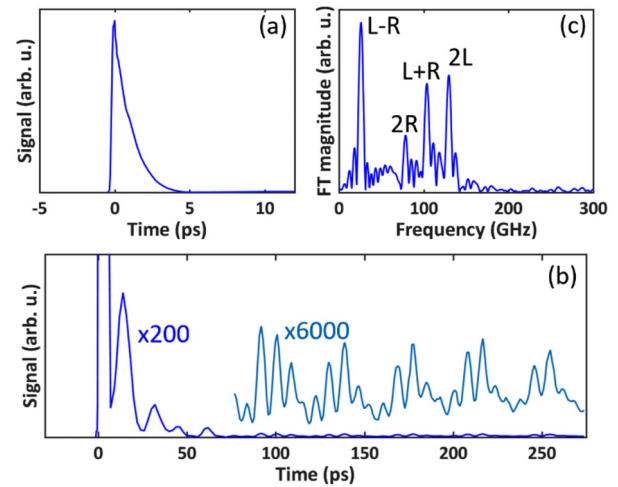


FIG. 2. (a) Diffraction signal vs pump-probe time delay in transmission from single crystal diamond. (b) Same as (a), with a longer temporal range and the vertical scale stretched by a factor of 200 to make details in the tail of the signal discernible. Inset: oscillations in the tail of the signal enhanced by a factor of 6000 compared to (a). (c) Fourier spectrum of the oscillations in the inset in (b); the four peaks are harmonics and sum/difference frequencies of the longitudinal (L) and surface Rayleigh (R) waves.

the inset in Fig. 2(b). The amplitude of these oscillations is four orders of magnitude smaller than the initial peak,³¹ yet we were able to measure them with a good signal-to-noise ratio with averaging over 2000 FEL shots. The Fourier spectrum of the oscillations shown in Fig. 2(c) reveals four peaks, which are identified as second harmonics and sum/difference of the bulk longitudinal wave frequency 64.7 GHz and the Rayleigh SAW frequency 38.8 GHz. From the elastic constants of diamond,³² we calculated the acoustic velocities in the [110] direction, $c_L = 18360 \text{ m/s}$ and $c_R = 11150 \text{ m/s}$ for the longitudinal wave and SAW, respectively. The corresponding frequencies are equal to c_L/Λ and c_R/Λ , i.e., 66.3 and 40.3 GHz, respectively. A small systematic deviation between the calculated and observed frequencies is likely due to an error in θ .³³

The reason that the spectrum contains the harmonics and the combination frequencies only is that the diffraction signal is quadratic with respect to the refractive index change, and, consequently, with respect to the strain amplitude in the sample.²⁵ The intensity of the diffracted signal is given by

$$I = [S_e(t) + S_{th}(t) + A_L \cos(\omega_L t) + A_R \cos(\omega_R t)]^2, \quad (1)$$

where S_e and S_{th} are the contributions of non-propagating electronic and thermal responses, and the third and fourth terms represent the contributions of the bulk longitudinal waves and SAWs, respectively. After the electronic and thermal responses have fully decayed, only the third and fourth terms in brackets are left: from that point on, the signal only contains harmonics and combination frequencies $2\omega_L$, $2\omega_R$, $\omega_L + \omega_R$, and $\omega_L - \omega_R$. Based on Fig. 2(b), we believe that the thermal grating (i.e., the periodic temperature variation) still contributes to the signal up to $\sim 60 \text{ ps}$. While the heat equation yields a thermal grating decay time of $\sim 1.6 \text{ ps}$, thermal transport in diamond at $\sim 100 \text{ nm}$ scale is expected to be slower than the Fourier law predicts.³⁴ Indeed, in 1.6

ps, thermal phonons in diamond cannot propagate farther than 1/10 of the TG period.

A simultaneous observation of laser-generated bulk and surface acoustic waves in bulk samples is uncommon: typically, experiments are either conducted on weakly absorbing or transparent samples at both pump and probe wavelengths, in which case, only bulk acoustic waves are observed,^{18,19,25} or on opaque samples yielding only SAWs.^{23,24} In our case, the sample is opaque for the excitation but transparent for the probe. The usefulness of simultaneous measurements of bulk longitudinal and SAW velocities for characterizing the elastic properties of materials has already been demonstrated in experiments where metal nanostructures were used to generate SAWs.^{10,35}

Figure 3(a) shows the signal measured in transmission on the BK-7 sample. The initial electronic response peak¹² is not resolved due to the large (5 ps) probe delay step size. The dominant oscillation frequency of 21.9 GHz is close to the expected longitudinal acoustic frequency of 21.8 GHz.³⁶ A Fourier-spectrum of the data shown in Fig. 3(b) reveals a smaller peak at 11.7 GHz close to the expected SAW frequency 12.1 GHz.³⁶ The reason we do not see harmonics and combination frequencies is that the thermal diffusivity of BK-7 is low and the estimated thermal grating decay time is ~ 4 ns. Consequently, S_{th} is almost constant on the time scale of the measurement, and the signal is dominated by the terms $S_{th}A_L \cos(\omega_L t)$ and $S_{th}A_R \cos(\omega_R t)$.

Figures 3(c) and 3(d) show the signal and the corresponding Fourier spectrum obtained in the reflection mode from the same sample and simultaneously with the signal recorded in transmission. Now the SAW peak is more prominent, and an additional peak appears at 47.2 GHz. The origin of this peak is explained by considering the phase matching conditions for diffraction of the probe beam by bulk acoustic waves in the transmission and reflection modes. Since the excitation light is absorbed in a thin subsurface layer, the acoustic wavevector component along the surface normal q_z

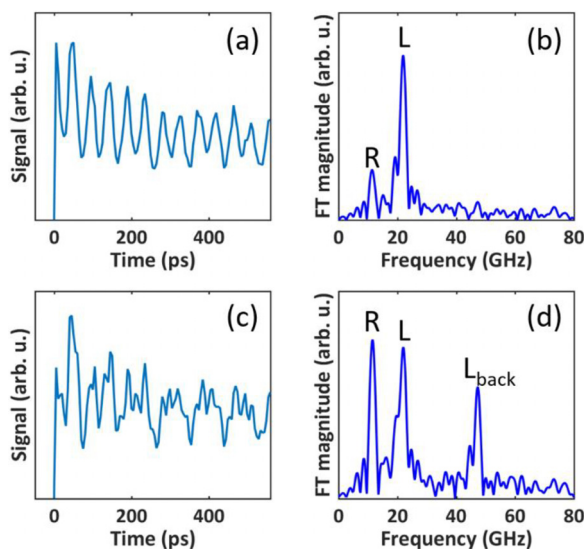


FIG. 3. Measurements on BK-7 glass. (a) Diffraction signal vs probe pulse delay in transmission and (b) the corresponding Fourier spectrum. (c) Diffraction signal in reflection and (d) the corresponding spectrum. Spectral peaks correspond to the Rayleigh SAW (R) and to bulk longitudinal waves yielding forward- (L) and back-scattering (L_{back}) diffraction.

is not precisely defined; rather, we generate acoustic waves with a broad spectrum of q_z . By contrast, the wavevector component along the surface is strictly set by the excitation interference pattern period, $q_x = 2\pi/\Lambda$. In this case, there are two values of q_z , at which the phase matching condition is satisfied (see the derivation in the [supplementary material](#)): (i) $q_z = 0$, which yields diffraction in the forward direction and (ii) $q_z = 2k\sqrt{1 - q_x^2/4k^2}$, where $k = 2\pi n/\lambda_p$ is the optical wavevector in the medium, and n is the refractive index, yielding diffraction in the backscattering direction, with the modulus of the acoustic wavevector equal to $q = 2k = 4\pi n/\lambda_p$. The expected acoustic frequency in the back-scattered signal is $2nc_L/\lambda_p = 46.4$ GHz, close to the observed value. The presence of the 21.9 GHz peak in the back-scattered signal can be explained by the reflection of the forward-scattered signal from the back surface of the sample.

Figure 4 presents data from BGO. The thermal conductivity of BGO is low enough³⁷ to yield a slow thermal decay. Acoustic oscillations seen in Fig. 4(a) yield a Fourier spectrum resembling that obtained on BK-7, with the longitudinal peak at 14.3 GHz and Rayleigh surface wave peak at 7.9 GHz, see Fig. 4(b); reflection-mode data (see [supplementary material](#)) also show trends similar to BK-7. Of particular interest is the initial fast dynamics shown in Fig. 4(c) revealing oscillations at 2.84 THz and yielding a corresponding peak in the Fourier spectrum shown in Fig. 4(d). BGO is known to have a strong A_1 optical phonon mode often observed in optical pump-probe experiments,^{38,39} whose frequency is reported to be 2.76 THz⁴⁰ or 2.68 THz.³⁸ The slightly higher observed frequency might be explained by the interference with the 2.95 THz mode.³⁸ (Measurements at longer delays—not conducted due to the beamtime constraints—would reveal whether the apparent oscillations decay is due to the beating between the two modes.) The TG wavevector is too small to affect the optical phonon frequency; that is, we effectively observe the zone-center phonon.

In optical pump-probe measurements,^{38,39} the 2.7 THz phonon mode in BGO is excited via Impulsive Stimulated

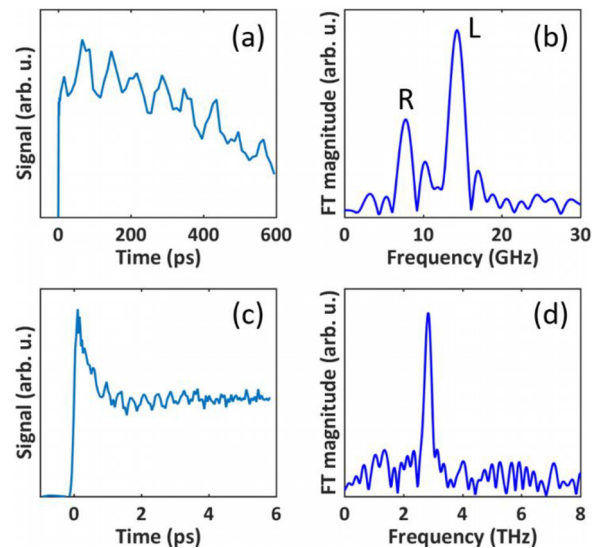


FIG. 4. (a) Diffraction efficiency in transmission vs probe delay and (b) the corresponding Fourier spectrum for BGO; (c) The onset of the signal acquired with an enhanced temporal resolution and (d) the corresponding Fourier spectrum.

Raman Scattering (ISRS).⁴¹ However, the ISRS mechanism is unlikely to work with EUV excitation for two reasons: (i) ISRS measurements are typically done in transparent media (for both pump and probe). For the EUV pump, the penetration depth into BGO is only 28 nm. Since the ISRS signal is proportional to the square of the interaction length, the signal will be reduced by a factor of 10^6 or more compared to a typical optical experiment. (ii) The ISRS mechanism relies on the dependence of the polarizability on the phonon coordinate.³⁹ In the EUV range, the polarizability itself is smaller, and its dependence on the phonon coordinate is greatly smaller than in the visible range. Thus, we believe that the observed coherent optical phonon motion is driven by the electronic excitation via the displacive mechanism⁴² rather than by ISRS.

On the other hand, the mechanisms of the excitation of coherent acoustic phonons are likely to be similar to the case of the optical excitation of opaque media.⁴³ The most universal mechanism is thermal expansion: the thermoelastic excitation of coherent acoustic phonons requires that a significant part of the excitation energy be transferred to the thermal phonon system faster than in half-period of the acoustic phonon. Since the acoustic period in our experiments is relatively long (15–100 ps), this requirement is easily met. Acoustic waves can also be produced by photoexcited carriers via the deformational potential mechanism,⁴³ which may be important for diamond due to its low thermal expansion coefficient. The elucidation of the dominant mechanism for each material goes beyond the scope of this report.

In conclusion, we have demonstrated the excitation of coherent acoustic and optical phonons by coherent femtosecond EUV pulses in the transient grating geometry. Currently, the capabilities of the TG experiment are still limited by the use of the optical probe: we can excite acoustic waves with smaller wavelengths but the optical probe cannot detect them. However, the acoustic frequencies we are able to generate are already quite high: for example, surface acoustic waves with frequencies higher than ~ 5 GHz²⁰ could previously be generated only with the help of nanoscale periodic structures.^{9,44} Thus, even within the currently accessible wavevector range, one can greatly expand the capabilities of SAW spectroscopy. For example, even for such a practically important SAW material as LiNbO₃, the attenuation has only been measured up to 5 GHz for SAWs⁴⁵ and up to 10 GHz for bulk waves.⁴⁶

The implementation of the EUV probe will be the next step in the development of the EUV TG technique. With the FERMI FEL wavelength range 4–100 nm, it would be possible to excite acoustic waves with a wavelength tunable from single-digit nanometers to a few microns, covering GHz to THz frequencies.⁴⁷ Since all materials are highly absorbing in the EUV range, one can excite acoustic waves in any material without metal film transducers, which are often used to generate high frequency acoustic waves with optical pulses.^{4,9,10,42} An intriguing question is whether coherent phonons across the entire Brillouin zone can be generated using even shorter (soft or hard x-ray) wavelengths. Whether EUV excitation of coherent optical phonons will also open

new opportunities remains to be seen: a further study beyond the initial observation reported here is needed.

It should also be mentioned that the data quality and the ability to resolve fine features of the signal, demonstrated, for example, by Fig. 2, significantly exceed those typical for time-resolved EUV pump/optical probe measurements,^{15–17} indicating the advantage of the background-free TG experiment, in which the diffracted optical signal vanishes in the absence of the EUV excitation. Our results indicate the promise of the TG technique for studying a wide range of phenomena initiated by femtosecond EUV pulses.

See [supplementary material](#) for the details of obtaining a complete signal waveform from separate scans on diamond, the derivation of acoustic phonon wavevectors probed in transmission and reflection geometries, and reflection-mode measurements on BGO.

The contribution by the MIT group was supported by the U.S. Department of Energy, Office of Basic Energy Sciences under Award No. DE-FG02-00ER15087. The JILA group graciously acknowledges support from the Department of Energy BES Award No. DE-FG02-99ER14982 and the Gordon and Betty Moore Foundation's EPiQS Initiative through Grant No. GBMF: 4538, and J.K. acknowledges support from an SRC Fellowship. The Elettra group acknowledges the European Research Council Grant No. 202804-TIMER. A.C. and T.F. acknowledge the Swiss NSF through the NCCR-MUST.

¹D. Attwood and A. Sakdinawat, *X-Rays and Extreme Ultraviolet Radiation: Principles and Applications* (Cambridge University Press, Cambridge, 2016).

²C. Rose-Petrucci, R. Jimenez, T. Guo, A. Cavalleri, C. W. Siders, F. Rksi, J. A. Squier, B. C. Walker, K. R. Wilson, and C. P. J. Barty, *Nature* **398**, 310 (1999).

³M. Bargheer, N. Zhavoronkov, Y. Gritsai, J. C. Woo, D. S. Kim, M. Wörner, and T. Elsaesser, *Science* **306**, 1771 (2004).

⁴A. Bojahr, M. Gohlke, W. Leitenberger, J. Pudell, M. Reinhardt, A. von Reppert, M. Roessle, M. Sander, P. Gaal, and M. Bargheer, *Phys. Rev. Lett.* **115**, 195502 (2015).

⁵T. Henighan, M. Trigo, S. Bonetti, P. Granitzka, D. Higley, Z. Chen, M. P. Jiang, R. Kukreja, A. Gray, A. H. Reid *et al.*, *Phys. Rev. B* **93**, 220301 (2016).

⁶K. Sokolowski-Tinten, C. Blome, J. Blums, A. Cavalleri, C. Dietrich, A. Tarasevitch, I. Uschmann, E. Förster, M. Kammler, M. Horn-von-Hoegen *et al.*, *Nature* **422**, 287 (2003).

⁷S. L. Johnson, P. Beaud, E. Möhr-Vorobeva, A. Caviezel, G. Ingold, and C. J. Milne, *Phys. Rev. B* **87**, 054301 (2013).

⁸M. Trigo, M. Fuchs, J. Chen, M. P. Jiang, M. Cammarata, S. Fahy, D. M. Fritz, K. Gaffney, S. Ghimire, A. Higginbotham *et al.*, *Nat. Phys.* **9**, 790 (2013).

⁹M. E. Siemens, Q. Li, M. M. Murnane, H. C. Kapteyn, R. Yang, E. H. Anderson, and K. A. Nelson, *Appl. Phys. Lett.* **94**, 093103 (2009).

¹⁰J. N. Hernandez-Charpak, K. M. Hoozeboom-Pot, Q. Li, T. D. Frazer, J. L. Knobloch, M. Tripp, S. W. King, E. H. Anderson, W. Chao, M. M. Murnane *et al.*, *Nano Lett.* **17**, 2178 (2017).

¹¹S. M. Durbin, T. Clevenger, T. Graber, and R. Henning, *Nat. Photonics* **6**, 111 (2012).

¹²F. Bencivenga, R. Cucini, F. Capotondi, A. Battistoni, R. Mincigrucci, E. Giangrisostomi, A. Gessini, M. Manfredda, I. P. Nikolov, E. Pedersoli *et al.*, *Nature* **520**, 205 (2015).

¹³I. Inoue, Y. Inubushib, T. Sato, K. Tono, T. Katayama, T. Kameshima, K. Ogawa, T. Togashi, S. Owada, Y. Amemiya *et al.*, *PNAS* **113**, 1492 (2016).

- ¹⁴E. Ferrari, C. Spezzani, F. Fortuna, R. Delaunay, F. Vidal, I. Nikolov, P. Cinquegrana, B. Diviacco, D. Gauthier, G. Penco *et al.*, *Nat. Commun.* **7**, 10343 (2016).
- ¹⁵F. Bisio, E. Principi, M. Magnozzi, A. Simoncig, E. Giangrisostomi, R. Mincigrucchi, L. Pasquali, C. Masciovecchio, F. Boscherini, and M. Canepa, *Phys. Rev. B* **96**, 081119 (2017).
- ¹⁶F. Tavella, H. Höppner, V. Tkachenko, N. Medvedev, F. Capotondi, T. Golz, Y. Kai, M. Manfreda, E. Pedersoli *et al.*, *High Energy Density Phys.* **24**, 22 (2017).
- ¹⁷A. Simoncig, R. Mincigrucchi, E. Principi, F. Bencivenga, A. Calvi, L. Foglia, G. Kurdi, A. Matruggio, S. Dal Zilio, V. Masciotti *et al.*, *Phys. Rev. Mater.* **1**, 073802 (2017).
- ¹⁸H. J. Eichler, P. Günter, and D. Pohl, *Laser-Induced Dynamic Gratings* (Springer-Verlag, Berlin, 1986).
- ¹⁹K. A. Nelson, R. J. D. Miller, D. R. Lutz, and M. D. Fayer, *J. Appl. Phys.* **53**, 1144 (1982).
- ²⁰J. A. Rogers, A. A. Maznev, M. J. Banet, and K. A. Nelson, *Annu. Rev. Mater. Sci.* **30**, 117 (2000).
- ²¹N. Boechler, J. K. Eliason, A. Kumar, A. A. Maznev, K. A. Nelson, and N. Fang, *Phys. Rev. Lett.* **111**, 036103 (2013).
- ²²M. Sander, M. Herzog, J. E. Pudell, M. Bargheer, N. Weinkauff, M. Pedersen, G. Newby, J. Sellmann, J. Schwarzkopf, V. Besse *et al.*, *Phys. Rev. Lett.* **119**, 075901 (2017).
- ²³R. A. Duncan, F. Hofmann, A. Vega-Flick, J. K. Eliason, A. A. Maznev, A. G. Every, and K. A. Nelson, *Appl. Phys. Lett.* **109**, 151906 (2016).
- ²⁴J. Janušonis, C. L. Chang, P. H. M. van Loosdrecht, and R. I. Tobey, *Appl. Phys. Lett.* **106**, 181601 (2015).
- ²⁵A. R. Duggal and K. A. Nelson, *J. Chem. Phys.* **94**, 7677 (1991).
- ²⁶F. Bencivenga, A. Calvi, F. Capotondi, R. Cucini, R. Mincigrucchi, A. Simoncig, M. Manfreda, E. Pedersoli, E. Principi, F. Dallari *et al.*, *Faraday Discuss.* **194**, 283 (2016).
- ²⁷F. Capotondi, E. Pedersoli, F. Bencivenga, M. Manfreda, N. Mahne, L. Raimondi, C. Svetina, M. Zangrando, A. Demidovich, I. Nikolov *et al.*, *J. Synchrotron Radiat.* **22**, 544 (2015).
- ²⁸E. Allaria, D. Castronovo, P. Cinquegrana, P. Craievich, M. Dal Forno, M. B. Danailov, G. D'Auria, A. Demidovich, G. De Ninno, S. Di Mitri *et al.*, *Nat. Photonics* **7**, 913 (2013).
- ²⁹The width of the interference pattern at the sample is limited by $L_c/\sin(\theta)$, where L_c is the coherence length of the FEL pulse. For a transform-limited 70 fs-long pulse L_c is $\sim 20 \mu\text{m}$; consequently, at the crossing angle used in our experiment, the interference pattern can be as wide as $\sim 0.9 \text{ mm}$.
- ³⁰B. L. Henke, E. M. Gullikson, and J. C. Davis, *At. Data Nucl. Data Tables* **54**, 181 (1993).
- ³¹The initial peak was measured at a five times smaller EUV energy to avoid the saturation of the detector, and at a smaller CCD integration time than the tail of the signal. The complete signal waveform was then obtained by stitching three experimental traces by matching the overlapping parts of the waveform, see supplementary material.
- ³²A. Migliori, H. Ledbetter, R. G. Leisure, C. Pantea, and J. B. Betts, *J. Appl. Phys.* **104**, 053512 (2008).
- ³³From the measured acoustic frequencies, we get a corrected value of 2θ equal to 2.55° , which is 3% smaller than the set value. With this corrected angle, the calculated longitudinal and Rayleigh wave frequencies are 64.3 and 39.0 GHz, respectively, i.e., within 0.6% from the measured frequencies. However, we could not apply the corrected value of θ to measurements on other samples, as the setup was realigned between the measurements.
- ³⁴J. A. Johnson, A. A. Maznev, J. Cuffe, J. K. Eliason, A. J. Minnich, T. Kehoe, C. M. Sotomayor Torres, G. Chen, and K. A. Nelson, *Phys. Rev. Lett.* **110**, 025901 (2013).
- ³⁵P. A. Mante, J. F. Robillard, and A. Devos, *Appl. Phys. Lett.* **93**, 071909 (2008).
- ³⁶From the properties of BK-7 listed by Shott, density 2.51 g/cm^3 , Young's modulus 82 GPa, Poisson's ratio 0.206, we obtain longitudinal and Rayleigh velocities of 6048 m/s and 3356 m/s, respectively.
- ³⁷H. Shen, J.-Y. Xu, W.-J. Ping, Q.-B. He, Y. Zhang, M. Jin, and G.-J. Jiang, *Chin. Phys. Lett.* **29**, 076501 (2012).
- ³⁸Z. Chen, Y. Gao, B. C. Minch, and M. F. DeCamp, *J. Phys.: Condens. Matter* **23**, 385402 (2011).
- ³⁹J. K. Wahlstrand, R. Merlin, X. Li, S. T. Cundiff, and O. E. Martinez, *Opt. Lett.* **30**, 926 (2005).
- ⁴⁰M. Couzi, J. R. Vignalou, and G. Boulon, *Solid State Commun.* **20**, 461 (1976).
- ⁴¹Y.-X. Yan, E. B. J. Gamble, and K. A. Nelson, *J. Chem. Phys.* **83**, 5391 (1985).
- ⁴²H. J. Zeiger, J. Vidal, T. K. Cheng, E. P. Ippen, G. Dresselhaus, and M. S. Dresselhaus, *Phys. Rev. B* **45**, 768 (1992).
- ⁴³P. Ruello and V. E. Gusev, *Ultrasonics* **56**, 21 (2015).
- ⁴⁴D. H. Hurley and K. L. Telschow, *Phys. Rev. B* **66**, 153301 (2002).
- ⁴⁵A. J. Slobodnik, Jr., P. H. Carr, and A. J. Burdeau, *J. Appl. Phys.* **41**, 4380 (1970).
- ⁴⁶I. L. Bajak, A. McNab, J. Richter, and C. D. W. Wilkinson, *J. Acoust. Soc. Am.* **69**, 689 (1981).
- ⁴⁷The range of phonon frequencies that can be excited is also limited by the excitation EUV pulse duration. With 70 fs FEL pulses, phonon frequencies up to $\sim 7 \text{ THz}$ can be generated.